Journal of Solid State Chemistry 184 (2011) 536–545

Contents lists available at ScienceDirect

Journal of Solid State Chemistry

journal homepage: www.elsevier.com/locate/jssc

Ferromagnetism and antiferromagnetism coexistence in $SrRu_{1-x}Mn_xO_3$: Density functional calculation

H. Hadipour, S. Fallahi, M. Akhavan *

Magnet Research Laboratory (MRL), Department of Physics, Sharif University of Technology, P.O. Box 11365-9161, Tehran, Iran

ARTICLE INFO

Article history:
Received 7 August 2010
Received in revised form
22 December 2010
Accepted 3 January 2011
Available online 7 January 2011

Keywords:
Ruthenates
Ferromagnetic materials
Double exchange

ABSTRACT

We have calculated the electronic structure of $SrRu_{1-x}Mn_xO_3$ using the full potential linearized augmented plane wave method by LSDA and LSDA+U. The antiparallel alignment between the Mn and Ru ions are consistent with the competition between ferromagnetism and antiferromagnetism in the low Mn-doped polycrystalline samples. This is in contrast to the appearance of quantum critical point and FM and AFM transitions in the single crystal measurement. Our results show that the discrepancy between different experimental phase diagrams is related to the conditions of sample preparation and also the difference between the degree of magnetic interactions between the Mn and Ru moments. The DOS and the calculated Mn magnetic moment is similar to the magnetic moment of a purely ionic compound with d^3 configuration. The AFM state has band gap of 1.2 eV at the Fermi energy predicting an insulating behavior.

1. Introduction

The orbital and spin ordering displayed by many transition metal oxides like ruthenates indicate the fundamental role of electron correlation in these materials [1–3]. Substituting the 4*d* ions by the 3*d* impurity ions extensively changes the magnetic ground state accompanied by a metal–insulator transition. Ru 4*d* orbitals is more extended as compared to those of 3*d* ions which changes the crystalline electric fields (CEF), *p*–*d* hybridization, exchange energy, electron–electron correlation, and so on in the ruthenates.

Creation of the Ru site vacancies in $SrRuO_3$, and doping with foreign elements in $SrRu_{1-x}M_xO_3$ (M=Mg [4,5], Fe [6], Ti [7–10], Zn [11], Ni [11], Co [11]) significantly decreases the Curie temperature T_C, whereas doping with Cr [11–15] and Pb [16] increases T_C up to 185 K. One of the most important phenomena among these elements appear when Mn is substituted for Ru in the $SrRu_{1-x}M_xO_3$ oxide [17–19]. $SrRuO_3$ is an itinerant ferromagnet (FM) with T_C=165 K with the saturation moment between 0.8 and 1.6μ_B/Ru [16,14,20,21]. The crystal electric field in the Ru^{4+} $4d^4$ ions is so large, yielding a low spin state with S=1. The perovskite $SrMnO_3$ having only the Mn^{4+} $3d^3$ ions, is an insulator, and has cubic symmetry with the t_{2g} spins ($S=\frac{3}{2}$) ordering antiferromagnetically in the *G*-type phase [22–24]. In $SrMnO_3$, the 3*d* t_{2g} electrons are localized and the interaction among the t_{2g} electrons on the neighboring Mn ions is via antiferromagnetic (AFM) superexchange mediated by the O bonds.

Cao et al. have shown that increasing Mn-doping in the single crystal samples drives $SrRu_{1-x}Mn_xO_3$ from the itinerant FM state through a quantum critical point (QCP) at x_c=0.39, to an insulating AFM state [17]. A Mott-type transition and QCP feature at the composition x_c divides the FM metal from the AFM insulator. This significant decrease of T_C is similar to the case of doping Ca at the Sr site [25] or Ti and Mg doping at the Ru site [9,4,5]. Their magnetization studies show that Mn is substituted as Mn^{4+}, while Ru remains as Ru^{4+}, far from Ru^{5+} ($S=\frac{3}{2}$) along with Mn^{3+} (S=2). Some contradictory findings from the single crystal results of Ref. [17] have been obtained by other works on the polycrystalline samples. Sahu et al. [18,26] have reported that the FM state may still be observed with higher Mn contents in $SrRu_{0.5}M_{0.5}O_3$. They observed only a marginal decrease of 40 K in T_C for 50% of Mn-doping, in contrast to the drastic reduction of T_C reported for single crystal in the Cao et al. experimental results [17]. Also, Zheng et al. have shown that ferromagnetism is retained in the polycrystalline samples until Mn-doping reaches 0.61 [27]. Also, the results from most of the experiments like X-ray absorption spectroscopy and magnetization suggest the existence of the mixed valence states (Mn^{3+}/Mn^{4+} and Ru^{4+}/Ru^{5+}) for polycrystalline $SrRu_{1-x}Mn_xO_3$ samples [24,19]. Recently, Horiba et al. have performed both X-ray photoemission spectroscopy and X-ray absorption spectroscopy to study the electronic state of the polycrystalline $SrRu_{1-x}Mn_xO_3$. The Mn substitution in $SrRuO_3$ decreases the magnetization, and ferromagnetism disappears around x=0.3 [19].

* Corresponding author. Fax: +98 21 66012983.
E-mail address: akhavan@sharif.edu (M. Akhavan).

0022-4596/$ - see front matter © 2011 Elsevier Inc. All rights reserved.
doi:10.1016/j.jssc.2011.01.007

In the single crystal $SrRu_{1-x}Mn_xO_3$, substitution of Ru by Mn disappears the metallic and FM character of the $RuSrO_3$ compound and also interrupts the dynamics of the Ru 4*d* t_{2g} electrons with increasing *x* [17]. Due to the mixed valence of Mn and Ru in polycrystalline samples, the double exchange (DE) FM interaction between $Mn^{3+}(t_{2g}^3\ e_g^1)$ and $Mn^{4+}(t_{2g}^3\ e_g^0)$ or $Ru^{5+}(t_{2g}^3\ e_g^0)$ competes with the AFM interaction between the two Mn ions. This behavior is similar as in $La_{0.5}Sr_{0.5}Ru_{1-x}Mn_xO_3$, where the Ru ions exist mainly in the form of Ru^{4+} with a small quantity of Ru^{5+} [28]. The marginal decrease of ferromagnetism is attributed to the FM exchange interaction between Mn^{3+} and $Ru^{4+}(Ru^{5+})$. Also, due to DE interaction, the magnetoresistance (MR) ratio (about 30% at Curie temperature $T_C = 125$ K) of $SrRu_{0.5}Mn_{0.5}O_3$ is two times higher than that of the parent compound $SrRuO_3$ [18].

In addition, by the nuclear magnetic resonance and neutron diffraction measurements in polycrystalline compounds, Yokoyama et al. [29] have indicated that there is a coexistence of FM interaction between the Mn ions, and AFM coupling between the Mn and Ru moments below the Curie temperature, which is different from sharp transition between FM to AFM according to QCP in the single crystal compounds. Zheng et al. have shown a complex phase diagram with coexistence of FM and AFM phases and a large MR by Mn substitution in polycrystal $SrRu_{1-x}Mn_xO_3$. Also, in the low and high Mn-doping, Ref. [24] has respectively obtained the FM and AFM phases, but the intermediate substitution ($0.2 < x < 0.4$) have a spin glass behavior instead of QCP behavior reported previously for single crystals [17]. Also, the spin glass behavior is attributed to the competition between ferromagnetism and antiferromagnetism gives rise to a large MR of 41% for the sample with $x=0.55$ [27,24].

This discrepancy may result from the difference between the single crystal and polycrystalline samples and the inhomogeneouity in polycrystalline compounds. One end member of the $SrRu_{1-x}Mn_xO_3$ family, $SrRuO_3$, have been described as crystallizing in the *Pbnm* orthorhombic, while $SrMnO_3$ has a *Pm*3*m* cubic space group symmetry. Ref. [24] shows that the symmetry changes from orthorhombic *Pbnm* for $x \le 0.2$ to tetragonal *I*4/*mcm* for $0.3 \le x \le 0.7$ to cubic *Pm*3*m* for $x \ge 0.8$ [24] by temperature-dependent neutron diffraction patterns for the $SrRu_{1-x}Mn_xO_3$ polycrystal. These results are different from the results of Refs. [17,26] (only Ref. [17] has produced single crystal), where the orthorhombic symmetry is retained as a function of *x*. In the single crystal samples, stability of the orthorhombic symmetries increases the threshold of site percolation of the nearest neighbor Ru–Ru bonds ($1-x_c$) with reducing both the dimensionality and FM coupling [17].

The questions that we address in this paper are thus the following: Which magnetic phase is stable in the low Mn-doping (about 25%) for the both orthorhombic and polycrystalline samples? What is the physical mechanism of the marginal decrease of the Curie temperature in $SrRu_{1-x}Mn_xO_3$ with *x* specially in polycrystalline compounds? Can localization of electrons overcome the FM coupling in the 50% of Mn substitution, which leads to the formation of AFM insulator? To answer these questions and what could influence the long-range FM coupling of $SrRuO_3$, we focus on the electronic contributions to the phase stability of the both low doping $SrMn_{0.25}Ru_{0.75}O_3$ compounds and high doping $SrMn_{0.5}Ru_{0.5}O_3$ compounds through the first-principles density functional theory. Depending on the space group of the structure, the computational results described in the low and high Mn-dopings is consistent with both the experimental results suggested in Ref. [24] with spin glass behavior, and also the phase diagram with QCP feature of Ref. [17].

2. Theoretical methods

The spin polarized electronic structure calculations for perovskite Mn-doped ruthenates $SrRu_{1-x}Mn_xO_3$ with $x=0.25$ and 0.50 is performed using the full-potential linearized augmented plane-wave (FLAPW) method [30] within the local spin density approximations (LSDA) and LSDA+*U* by WIEN2K software [31]. Additional local orbitals (LO) were used for all semicore states [32]. In the LSDA calculation we used the Perdew–Wang parameters for the exchange and correlation functional. The muffin-tin radii (RMT) for Sr, Ru, Mn, and O were set to 0.91, 0.90, 1.10, and 0.82 Å, respectively. The convergence for different calculations was achieved considering 500*k* points within the first Brillouin zone. The error bar for the energy convergence was set to 0.1 meV per formula unit.

In all calculations the lattice parameters were chosen to be equal to the refined computational lattice parameter (relaxed parameters) of $SrRu_{1-x}Mn_xO_3$ with both the *Pbnm* and *I*4/*mcm* space group. We have also carried out some of the calculations with the experimental lattice and atomic coordinates parameters (unrelaxed parameters), identical to those of both *Pbnm* and *I*4/*mcm* $SrRuO_3$ [33] and $SrRu_{1-x}Mn_xO_3$, but have not found any significant difference in the results. The atomic positions in the *Pbnm* symmetry (Fig. 1(a)) of $SrRuO_3$ used in these calculations are Sr:(0.0, 0.0130, 0.2500); Ru:(0.0, 0.0, 0.5); O(1):(0.0482, 0.4985, 0.2500); O(2):(0.2695, 0.2697, 0.0235). The atomic positions in the *I*4/*mcm* symmetry (Fig. 1(b)) of $SrRuO_3$ are Sr:(0.0, 0.5, 0.25); Ru:(0.0, 0.0, 0.5); O(1):(0.0, 0.0, 0.25); O(2):(0.25, 0.75, 0.0).

The dopants in $SrRu_{1-x}Mn_xO_3$ has been modeled by proper Mn substitutions for the Ru ions in the supercell approach under structure optimizations based on the refined lattice, both tetragonal *I*4/*mcm* and orthorhombic *Pbnm* structures. The $2\times2\times2$ crystallographic structures of the both orthorhombic *Pbnm* and tetragonal *I*4/*mcm* $SrRu_{1-x}Mn_xO_3$ ($x=0.25$) compounds are shown in Figs. 1(c) and 1(d), respectively. For every four Ru atoms one Ru is replaced by Mn, corresponding to 25% Mn substitution in a doubled cell $2\times2\times2$ of the computational structure of $SrRuO_3$. We have also calculated the electronic structures for both supercells, with the Mn moment parallel (P or FM alignments of Ru and Mn) and antiparallel (AP or AFM alignments of Ru and Mn) to the Ru magnetization (Figs. 2(a) and (b)). We have modeled competition of FM coupling between Ru atoms and AFM coupling between Ru–Mn atoms (similar to SG phase) in the AP alignment case. The Ru ions in the supercell have two configurations: Ru(1) with two Mn and four Ru neighbors and Ru(2) with six Ru neighbors.

In $SrRu_{0.5}Mn_{0.5}O_3$, we have used the Coulomb interaction between the localized Mn 3*d* and Ru 4*d* electrons in LSDA+*U*, whereas the interactions between the less localized *s* and *p* electrons are treated within LSDA. So, in the LSDA+*U* approach, introduced in Ref. [34], we add the orbital-dependent Coulomb interactions E_U to LSDA and subtract their average behavior (E_{dc}) to avoid double counting. Therefore, it can be written as the following:

$$E_{LSDA+U} = E_{LSDA} + E_U - E_{dc} \tag{1}$$

$$E_U = \frac{1}{2}\sum_{m,\sigma} \langle m,m''|V_{ee}|m',m'''\rangle \rho^{\sigma}_{m,m'}\rho^{-\sigma}_{m'',m'''} + (\langle m,m''|V_{ee}|m',m'''\rangle \tag{2}$$

$$-\langle m,m''|V_{ee}|m''',m'\rangle)\rho^{\sigma}_{m,m'}\rho^{\sigma}_{m'',m'''} \tag{3}$$

$$E_{dc} = \frac{1}{2}Un(n-1) - \frac{1}{2}J\sum_{\sigma} n^{\sigma}(n^{\sigma}-1) \tag{4}$$

where, $n = n^{\uparrow} + n^{\downarrow}$, $n_{\sigma} = Tr\rho^{\sigma}$, and V_{ee} is the screened Coulomb interactions among *d* electrons. We have used the fully localized limit (self-interaction corrected) approximation to introduce the double counting term in this work. The on-site Coulomb interaction strength of Mn is hard to determine precisely. The Coulomb

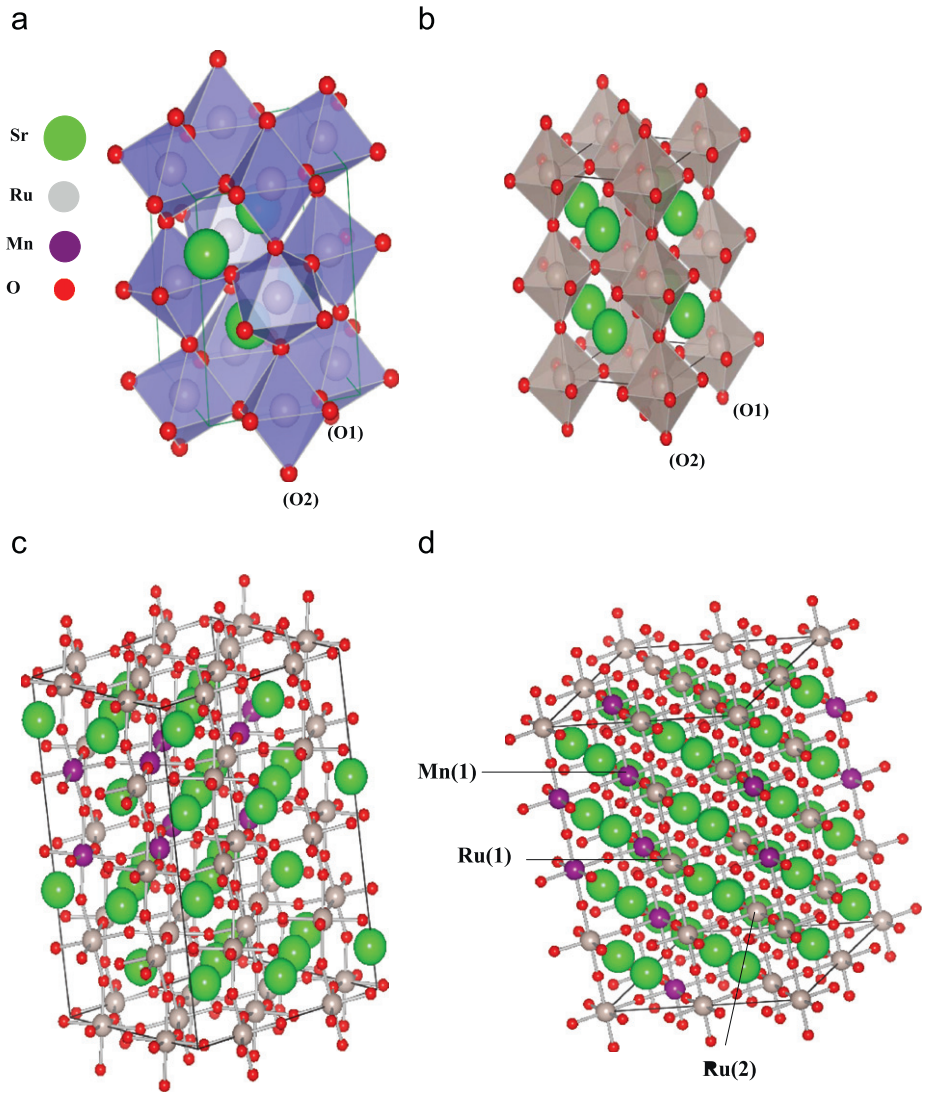

Fig. 1. Schematic diagram of the crystal structure of $SrMn_{0.25}Ru_{0.75}O_3$: (a) relaxed *Pbnm* space group of $SrRuO_3$, (b) relaxed *I*4/*mcm* space group of $SrRuO_3$, (c) relaxed *Pbnm* space group of supercell $SrMn_{0.25}Ru_{0.75}O_3$, (d) relaxed *I*4/*mcm* space group of supercell $SrMn_{0.25}Ru_{0.75}O_3$. O(1) represents the apical oxygen in the RuO_6 octahedra along the *z* axis in the structure and O(2) represents the oxygens in the basal *xy* plane. The thick solid lines show the Ru(Mn)–O–Ru(Mn) bands.

energy $U=5.5$ eV (Ref. [35]) and exchange parameter $J=1.6$ eV have been used for the Mn ions to explore the correlation effects in the 3*d* orbitals, whereas we have used $U=1.5$ eV for the Ru ions due to its nearly itinerant valence 4*d* orbitals.

3. Results and discussion

3.1. Low Mn-doping

Table 1 shows both the experimental and computational lattice parameters (*a*, *b*, and *c*), volume (*V*), and Ru–O–Ru bond angles for different crystal space group configurations of $SrRuO_3$, $SrRu_{0.75}Mn_{0.25}O_3$, and $SrRu_{0.5}Mn_{0.5}O_3$. The volume of the unit cell as well as the atomic coordinates for each configuration are optimized. For FM $x=0$ ($SrRuO_3$), the *Pbnm* configuration is stable with 0.52 eV/unit cell energy lower than *I*4/*mcm* configuration. The optimized lattice parameters with $|\Delta a|/a=0.87\%$, $|\Delta b|/b=0.27\%$, and $|\Delta c|/c=0.24\%$ are in good agreement with the experiment [33]. In $SrRu_{0.75}Mn_{0.25}O_3$, the total energy of *I*4/*mcm* configuration with AFM coupling of Mn and Ru is very close to the *Pbnm* configuration, having 0.05 eV/unit cell energy lower in the *I*4/*mcm* symmetry, which indicates that the boundary between the orthorhombic and tetragonal phase lies about $x=0.25$. The optimized unit cell dimensions for the both tetragonal *I*4/*mcm* and orthorhombic *Pbnm* structures of $SrRu_{0.75}Mn_{0.25}O_3$ are compared with the available experimental values in Table 1. The lattice parameters for both symmetries reduce with increasing *x* due to the smaller ionic radius of Mn as compared to Ru.

The calculated lattice parameters should decrease sharply for the charge balance of $Sr(Ru^{4+}_{1-x}Mn^{4+}_{x})O_3$ with increasing *x* (Mn^{4+} and Ru^{4+} with respective ionic radii of 0.52 and 0.63 Å). The experimental values of the lattice parameters for the *I*4/*mcm* symmetry presented in Table 1 show a slight decrease ($|\Delta V|/V=1.1\%$) with increasing *x* similar to our calculation for the tetragonal *I*4/*mcm* symmetry. In our calculation, the reduction of volume ($|\Delta V|/V$) are 2.7% and 0.7% for the *Pbnm* and *I*4/*mcm* space group, respectively. So, the *I*4/*mcm* symmetry are closer to the charge balance of $Sr(Ru^{4+,5+}_{1-x}Mn^{4+,3+}_{x})O_3$, and creation of Mn^{3+} and Ru^{5+} with respective ionic radii of 0.64 and 0.59 Å in the system.

As shown in Figs. 1(a) and (b), O(1) represents the apical oxygen in the RuO_6 octahedra along the *z* axis and O(2) is the oxygen in the basal *xy* plane. The experimental results show that increasing Mn reduces the structural distortion in the *I*4/*mcm* polycrystalline

system (increasing the Ru–O(2)–Ru bond angles from 164.05° to 166.17°) of the perovskite cell due to its smaller ionic radii as compared to Ru [24]. For both symmetries, our calculation is consistent with the experimental results [24] and with the marginal decrease of T_C with Mn substitution, which may be related to a smaller deviation of the Ru(Mn)–O–Ru(Mn) bond angle.

As we mentioned before, in polycrystalline samples, the symmetry changes from orthorhombic *Pbnm* to tetragonal *I*4/*mcm* around $x=0.2$–0.3 [24] with the existence of SG phase, different from the case of single crystal samples, where the orthorhombic symmetry is retained with increasing x [17]. The difference between the polycrystalline and single crystal samples considered for this calculation is the change of symmetry; and we have eliminated the effect of grain boundary, surface, and inhomogeneouity in our calculations. So, we first compare the two magnetic P (FM coupling of Ru and Mn) and AP (AFM coupling of Ru and Mn) phases in $SrRu_{0.75}Mn_{0.25}O_3$ for the tetragonal *I*4/*mcm* space group, and later will point out the results for the orthorhombic *Pbnm* symmetry.

3.1.1. Tetragonal polycrystalline samples of $SrRu_{0.75}Mn_{0.25}O_3$

The calculated DOS for the two end members of $SrRu_{0.75}Mn_{0.25}O_3$, namely, $SrRuO_3$ and $SrMnO_3$, have been shown in Figs. 3(a) and (b), respectively. As shown in Fig. 3(a), in the FM $SrRuO_3$, the Ru t_{2g} up-spin channel is completely occupied, while the Ru t_{2g} down-spin is partially occupied, consistent with the d^4 configuration of Ru. The CEF splitting ($E_{CEF}=E_{t_{2g\uparrow}}-E_{e_{g\uparrow}}\approx 1.1$ eV) in the Ru^{4+} $4d^4$ ions is comparable to the Ru exchange splitting ($E_{ES}=E_{t_{2g\uparrow}}-E_{t_{2g\downarrow}}\approx 1.0$ eV) due to the extension of the 4*d* orbitals. The higher number of electrons in the t_{2g} orbitals as compared with e_g orbitals shows that each of the four electrons occupy the t_{2g} orbitals, and there is low possibility to occupy the e_g orbitals in Ru^{4+}. The total density of states (TDOS) calculated for $SrMnO_3$ considered by the *G*-type AFM are presented in Fig. 3(b). Similar to Ref. [36], the ground state *G*-type AFM state for $SrMnO_3$ is found to be an insulator with a band gap of approximately 1.3 eV. It can also be noted that the AFM ground state has a Mn $3d^3$ configuration in the valence band.

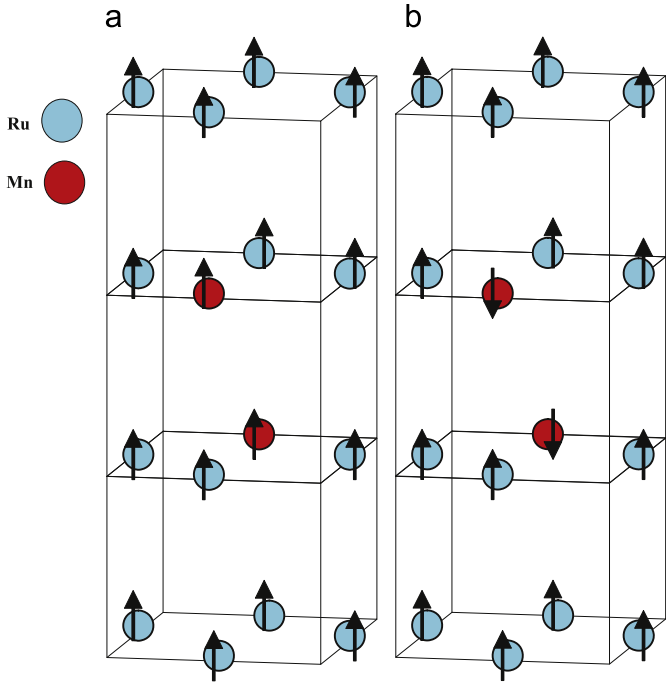

Fig. 2. Two magnetic configurations considered for *Pbnm* $SrMn_xRu_{1-x}O_3$: (a) parallel alignment of the Ru and Mn moments (P or FM alignments of Ru and Mn), (b) antiparallel alignment of the Ru and Mn moments (AP or AFM alignments of Ru and Mn).

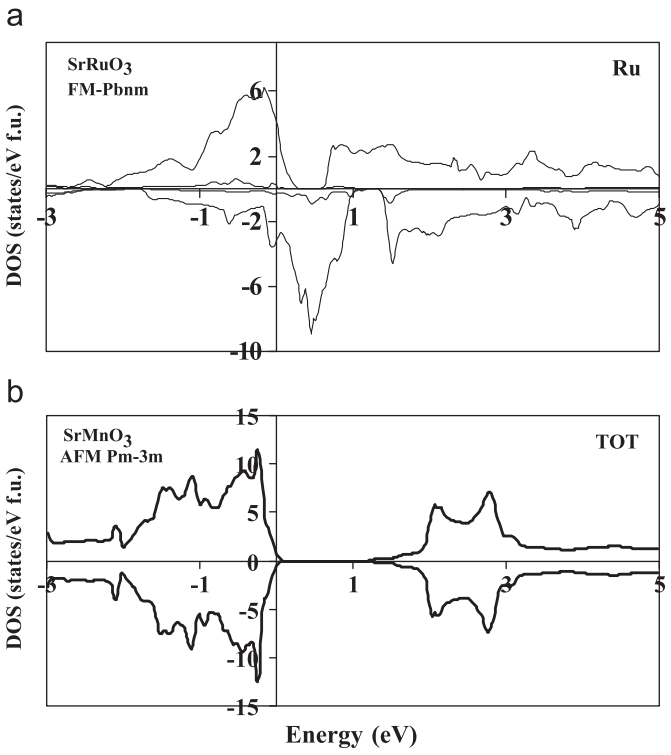

Fig. 3. (a) The Ru 4*d* DOS for FM $SrRuO_3$ in the orthorhombic *Pbnm* space group. (b) The total DOS (TDOS) for AFM $SrMnO_3$ in the cubic *Pm*3*m* space group.

Table 1
Unit cell dimensions (*a*,*b*, and *c*), volume (*V*) and Ru–O–Ru bond angles of both tetragonal *I*4/*mcm* and orthorhombic *Pbnm* space group of $SrRu_{1-x}Mn_xO_3$ perovskites.

Formula (space group)	*a* (Å)	*b* (Å)	*c* (Å)	*V* (Å^3)	Ru–O(1)–Ru	Ru–O(2)–Ru
Present computational work						
$SrRuO_3$ (*Pbnm*)	5.521	5.545	7.811	239.125	162.8	162.71
$SrRuO_3$ (*I*4/*mcm*)	5.571	5.571	7.848	243.570	180	164.05
$SrRu_{0.75}Mn_{0.25}O_3$ (*Pbnm*)	5.514	5.410	7.805	232.828	165.6	164.13
$SrRu_{0.75}Mn_{0.25}O_3$ (*I*4/*mcm*)	5.551	5.551	7.837	241.794	180	166.17
$SrRu_{0.5}Mn_{0.5}O_3$ (*I*4/*mcm*)	5.38	5.38	7.81	228.950	180	169.21
Experimental results						
$SrRuO_3$ (*Pbnm*) Refs. [17,33]	5.57	5.53	7.83	241.180	164.40	166.05
$SrRuO_3$ (*I*4/*mcm*) (T=823 K) Ref. [33]	5.57	5.57	7.907	246.141	180	168.35
$SrRu_{0.75}Mn_{0.25}O_3$ (*Pbnm*) Ref. [17]	5.54	5.47	7.82	236.975	–	–
$SrRu_{0.75}Mn_{0.25}O_3$ (*I*4/*mcm*) Ref. [24]	5.53	5.53	7.96	243.423	180	164
$SrRu_{0.5}Mn_{0.5}O_3$ (*I*4/*mcm*) Ref. [24]	5.40	5.40	7.90	230.364	180	168

The Ru and Mn DOS for the 25% Mn supercell with the P and AP alignment of Ru and Mn in the tetragonal *I*4/*mcm* are shown in Figs. 4(a)–(d). In order to investigate the contributions from various non-equivalent Ru and Mn sites, the Mn 3*d* DOS and Ru 4*d* DOS are plotted separately. We have only shown the shape of the Ru(1) DOS near the Mn(1) ion which depends on the Mn(1) moment direction. The Ru DOS with six Ru(2) neighbors for the low-doping $x=0.25$ case (not shown) are very similar to those of the undoped $SrRuO_3$. Due to the degeneracy of the t_{2g} orbitals in the both Ru and Mn atoms, only one of the t_{2g} orbitals (d_{xy}) is shown in the DOS result. And also, each of the Ru e_g orbitals have similar DOS distribution. In both cases, a metallic ground state is found to be stable and no energy gaps are observed in the DOS with strong Ru 4*d* and Mn 3*d* character at the Fermi level. The strong hybridization between Ru 4*d* and O 2*p* electronic contribution around E_F (not shown for simplicity) by increasing Mn in the low doping regime is consistent with the small measured lattice parameter and smaller ionic radius of Mn as compared to Ru.

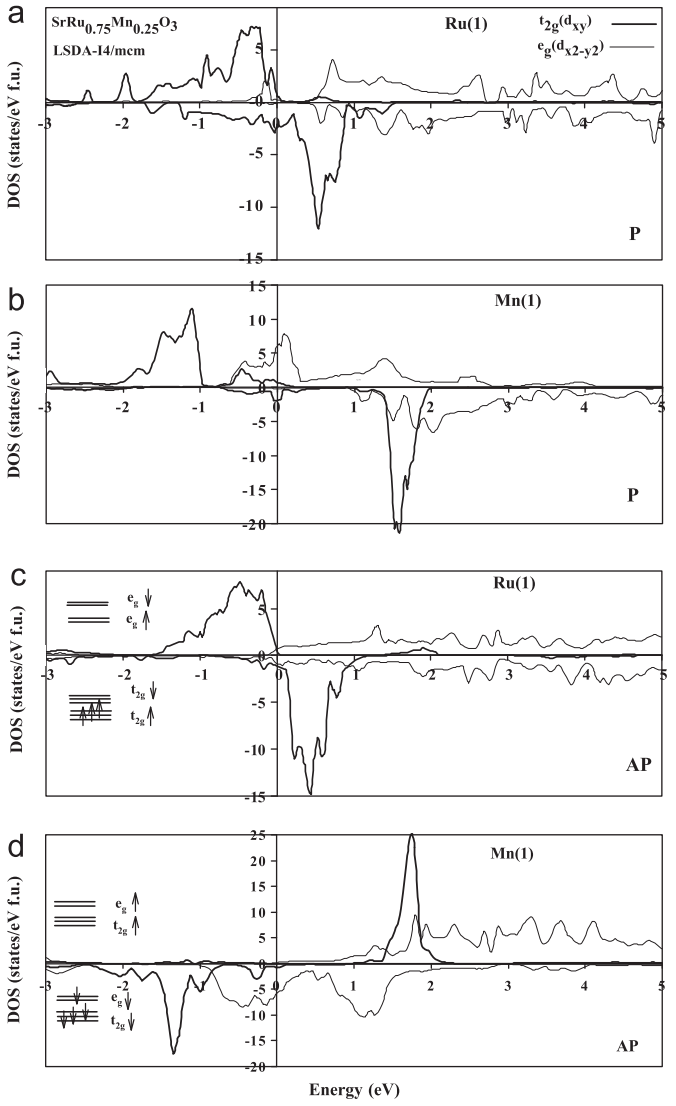

Fig. 4. DOS (d_{xy} and $d_{x^2-y^2}$) calculated by LSDA for $SrMn_{0.25}Ru_{0.75}O_3$ in the *I*4/*mcm* space group: (a) DOS of Ru(1) in the parallel alignment of Ru and Mn moments (P), (b) DOS of Mn(1) in the parallel alignment of Ru and Mn moments (P), (c) DOS of Ru(1) in the antiparallel alignment of Ru and Mn moments (AP), (d) DOS of Mn(1) in the antiparallel alignment of Ru and Mn moments (AP). The DOS results are presented for the two up- and down-spins.

The total energy of the *I*4/*mcm* configuration with AFM coupling of Mn and Ru is lower than FM coupling, and is assumed to be the stable phase. In spite of the lower energy of AP alignment calculation, we first point out the P alignment phase results for the tetragonal *I*4/*mcm* space group, and later compare this result with the AP alignment calculation. For the P alignment phase $SrRu_{0.75}Mn_{0.25}O_3$ (Figs. 4(a) and (b)), the main peaks of the up-spin and down-spin Ru(1) t_{2g} bands have significant mixing by the Mn 3*d* orbitals with the Ru E_{ES} and Ru E_{CEF} of 1.0 eV and 1.2 eV, respectively. Estimate of the Ru 4*d* occupation can be made by integrating the peak associated with the t_{2g} orbitals [37]. The occupied fraction of the peaks is 0.62, corresponding to an electron count of 3.7e, intermediate between $4d^4$ Ru^{4+} and $4d^3$ Ru^{5+}, but closer to $4d^4$ Ru^{4+}.

As may be seen from the DOS for $SrRu_{0.75}Mn_{0.25}O_3$, E_F in Fig. 4(b) occurs at the Mn up-spin e_g peak, while the up-spin t_{2g} peak starts below E_F. As shown in Table 2, the exchange energy $E_{ES}\approx 3$ eV aligning all spins of the Mn 3*d* electrons is relatively larger than $E_{CEF}\approx 0.6$ eV. The lower number of electrons in Ru t_{2g} in $SrRu_{0.75}Mn_{0.25}O_3$ as compared with Ru t_{2g} in $SrRuO_3$ shows that substitution of Ru by Mn replaces four itinerant 4*d* electrons with four localized 3*d* electrons. The orbital occupancy calculation by Mn e_g electrons shows that the Mn valence is between $3d^4$ Mn^{3+} and $3d^3$ Mn^{4+}, but closer to Mn^{4+}. So, the creation of Mn^{4+} and Ru^{4+} with small amount of Mn^{3+} and Ru^{5+} indicates less charge transfer between the Ru and Mn atoms (from Mn 3e in $x=1$ to Mn 3.4e in $x=0.25$ and Ru 4e in $x=0$ to Ru 3.7e in $x=0.25$) in the P alignment Mn low-doping calculation.

The mechanism for strong coupling between the Mn moment and the host $SrRuO_3$ is seen by comparing the P and AP alignment projections of the DOS. We have found that the energy difference between the Mn moments P and AP alignment to the $SrRuO_3$ host magnetization changes by 0.28 eV/unit cell, in favor of the AP alignment case. In Figs. 4(c) and (d), we have shown the DOS with AP alignment of Ru and Mn for $SrRu_{0.75}Mn_{0.25}O_3$ in the *I*4/*mcm* symmetry. The obtained DOS in Figs. 4(c) and (d) show the antiferromagnetic coupling and distinct orbital overlap between Ru and Mn in the tetragonal phase of $SrRu_{0.75}Mn_{0.25}O_3$. Also, we will see later that this Ru–Mn antiferromagnetic orbital overlap is higher in the tetragonal phase as compared to the orthorhombic phase. As shown in Fig. 4(c), the main difference with the P alignment is that the Ru t_{2g} down-spin and the Ru e_g up-spin are

Table 2
Electronic parameters for *I*4/*mcm* $SrRu_{1-x}Mn_xO_3$ perovskites deduced by DOS: crystalline electric field energy (E_{CEF}), exchange splitting (E_{ES}), Ru bandwidth (W).

Formula (approximation)	Ru (E_{CEF}) (eV)	Mn(E_{CEF}) (eV)	Ru(E_{ES}) (eV)	Mn(E_{ES}) (eV)	Rut_{2g} (W)	Mnt_{2g}(W) (eV)
$SrRuO_3$ (FM-LSDA)	1.1	–	1.0	–	2.2	–
$SrRu_{0.75}Mn_{0.25}O_3$ (P-LSDA)	1.2	0.6	1.0	3.0	2.0	1.0
$SrRu_{0.75}Mn_{0.25}O_3$ (AP-LSDA)	0.2	0.2	1.2	3.3	1.8	2.2
$SrRu_{0.75}Mn_{0.25}O_3$ (P-LSDA+U)	1.1	0.8	1.0	4.5	2.0	1.0
$SrRu_{0.75}Mn_{0.25}O_3$ (AP-LSDA+U)	0.2	0.3	1.2	3.3	2.0	2.1
$SrRu_{0.5}Mn_{0.5}O_3$ (P-LSDA)	0.1	0.1	1.2	3.2	1.5	1.50
$SrRu_{0.5}Mn_{0.5}O_3$ (AP-LSDA)	1.0	0.2	1.0	2.8	1.6	1.0
$SrRu_{0.5}Mn_{0.5}O_3$ (P-LSDA+U)	0.7	0.5	2.5	4.7	1.0	2.0
$SrRu_{0.5}Mn_{0.5}O_3$ (AP-LSDA+U)	2.2	0.2	2.5	4.8	1.0	1.0

Table 3
Electronic parameters for $I4/mcm$ $SrRu_{1-x}Mn_xO_3$ perovskites (only the $x=0$ calculation is derived by the *Pbnm* space group) deduced by the DOS: magnetic moment (MM), orbital occupancy (OO), total energy (E).

Formula (approximation)	Ru(MM) (μ_B)	Mn(MM) (μ_B)	Ru(OO) (e)	Mn(OO) (e)	E (eV)
$SrRuO_3$ (FM-LSDA)	1.16	–	4.0	–	0.00
$SrRu_{0.75}Mn_{0.25}O_3$ (P-LSDA)	1.27	2.90	3.7	3.4	0.28
$SrRu_{0.75}Mn_{0.25}O_3$ (AP-LSDA)	1.06	−3.27	3.1	3.7	0.0
$SrRu_{0.75}Mn_{0.25}O_3$ (P-LSDA+U)	1.06	3.27	4.0	3.1	0.00
$SrRu_{0.75}Mn_{0.25}O_3$ (AP-LSDA+U)	1.14	−3.18	3.1	4.0	0.4
$SrRu_{0.5}Mn_{0.5}O_3$ (P-LSDA)	1.4	2.92	3.5	3.2	0.18
$SrRu_{0.5}Mn_{0.5}O_3$ (AP-LSDA)	1.06	−3.0	3.2	3.8	0.0
$SrRu_{0.5}Mn_{0.5}O_3$ (P-LSDA+U)	1.64	3.33	3.0	3.8	0.16
$SrRu_{0.5}Mn_{0.5}O_3$ (AP-LSDA+U)	1.07	−3.4	3.0	3.2	0.0

near to the Fermi level, and lie in the same energy range. So, with the presence of Mn in the compound, the E_{ES} of the Ru t_{2g} electrons increases from 1.0 to 1.2 eV, while the energy separation between the Ru t_{2g} down-spin and the Ru e_g up-spin decreases from 0.5 to 0.1 eV.

Horiba et al. have obtained both the Ru and Mn valence states of $SrRu_{0.75}Mn_{0.25}O_3$ by PES measurement [19]. Our calculated DOS is consistent to the PES results that the intensity below E_F being reduced in the spectra of $SrRu_{0.75}Mn_{0.25}O_3$. Using the Ru 4d projection of the DOS, the filling of the Ru t_{2g} manifold decreases from 3.7e in the P alignment phase to 3.1e in the AP alignment phase (Table 3). From Figs. 4(c) and (d), it is evident that the Ru and Mn valence is closer to Ru^{5+} and Mn^{3+} than to Ru^{4+} and Mn^{4+}. There is apparently more charge transfer (from Mn 3e in $x=1$ to Mn 3.7e in $x=0.25$ and Ru 4e in $x=0$ to Ru 3.1e in $x=0.25$) between Mn and the ruthenate host as compared to the P alignment calculation which is consistent to the PES results [19]. This charge transfer eliminates one electron in the Ru 4d-shell, which would interrupt the itinerancy of the Ru electrons. The Ru up-spin t_{2g} and Mn down-spin e_g which are near to Fermi level, lie in the same energy range. This hybridization between the down-spin Mn e_g orbitals and up-spin Ru t_{2g} strongly favors AFM alignment of the Mn moments with the Ru host lattice magnetization. We have shown different e_g orbitals for the Mn atoms in Figs. 5(a) and (b) for P and AP alignment, respectively. Both Figs. 5(a) and (b) show that the $d_{z^2-3r^2}$ e_g orbitals lie close to E_F while the $d_{x^2-y^2}$ e_g orbitals spreads out above E_F. As seen in the Mn 3d projection of DOS, the Mn–Ru AFM alignment broadens both the down-spin Mn t_{2g} and e_g peaks and lowers the total energy.

We have achieved the magnetic moment value of $1.16\mu_B$/Ru for $SrRuO_3$ in the FM ordered state. As shown in Table 3, the spin magnetic moment of $SrRu_{0.75}Mn_{0.25}O_3$ centered at the Ru and Mn sites is found respectively to be about 1.27 and $2.9\mu_B$ in the P alignment calculation. The smaller Ru magnetic moment (≈ 1.06) and the higher Mn magnetic moment (≈ -3.27) are obtained by the AP alignment calculation as compared with the P alignment calculation for $SrRu_{1-x}Mn_xO_3$. Increasing the magnetic moment of Mn and reducing the magnetic moment of Ru in the AP alignment calculation agree with both the enhancement of effective PM moment [16,24,18,27,14] and the reduction of Ru ordered magnetic moment to 1.27 from $1.40\mu_B$ [14] for $SrRu_{0.9}Mn_{0.1}O_3$ at 50 kOe.

The stability of AP alignment calculation in the tetragonal $SrRu_{0.75}Mn_{0.25}O_3$ shows the coexistence of FM interaction

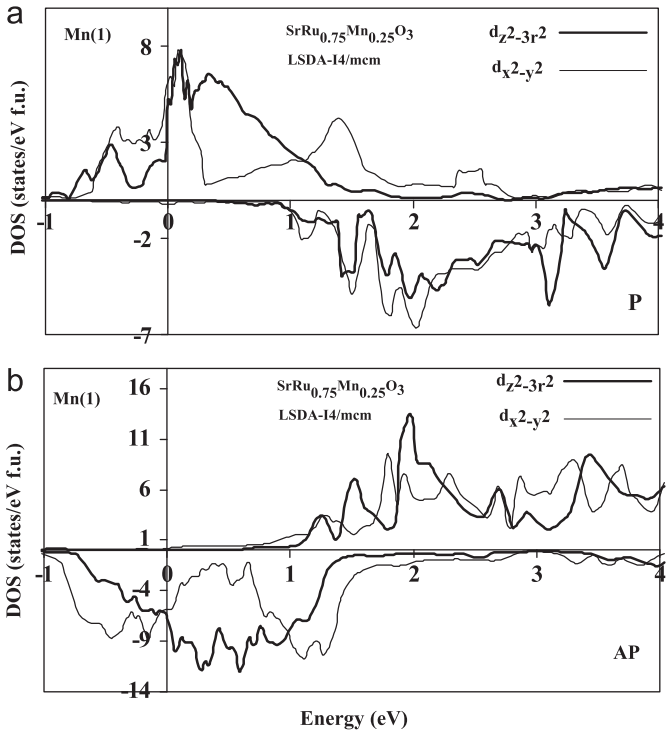

Fig. 5. DOS Mn 3d e_g orbitals calculated by LSDA for $SrMn_{0.25}Ru_{0.75}O_3$ in the $I4/mcm$ space group: (a) DOS of $d_{z^2-3r^2}$ and $d_{x^2-y^2}$ in the parallel alignment of the Ru and Mn moments (P), (b) DOS of $d_{z^2-3r^2}$ and $d_{x^2-y^2}$ in the antiparallel alignment of the Ru and Mn moments (AP).

between the Mn ions and AFM coupling between the Mn and Ru moments below the Curie temperature in the polycrystalline compounds which is consistent with the nuclear magnetic resonance and neutron diffraction measurements [29] and also Refs. [24,27] results. Retaining the high Curie temperature of the low Mn-doping is not because of the FM DE interaction between Mn^{3+} and Mn^{4+} or Ru^{5+}. The AFM hybridization between Mn and the Ru host lattice strongly favors the alignment of the Ru moments, and provides an explanation for the marginal decrease in the Curie temperature of $SrRuO_3$ with Mn substitution in the polycrystalline samples.

The hybridization of the Mn e_g and Ru t_{2g} orbitals has also been proposed in other studies [11,14]. This behavior is very similar to the effect of Cr^{3+} doping in $SrRu_{1-x}Cr_xO_3$ [37,12], and also the mechanism of high Curie temperature of Sr_2FeMoO_6 [38]. In $SrRu_{1-x}Cr_xO_3$, the decrease of the Ru magnetic moment and increase of the Curie temperature is attributed to the AP alignment coupling between the Cr and Ru ions [37,39]. In Sr_2FeMoO_6, due to hybridization with the Fe d^5 local moments, the Mo d orbital also becomes spin polarized, with an AFM alignment to the Fe moments. The DOS calculation (Figs. 4(c) and (d)) shows that substitution of Mn^{4+} for Ru^{4+} eliminates one electron in the d shell, and localizes the Ru electrons. The suppression of the FM ordering temperature in $SrRu_{1-x}Mn_xO_3$ is believed to be associated with localization of the Ru 4d electrons which competes with the enhancement of FM ordering due to AP alignment coupling between Mn and Ru. Therefore, the AP alignment between the Mn and Ru ions are consistent with formation of the spin glass phase in the polycrystalline samples [29,24,27], which is different from QCP between the FM and AFM transitions in single crystals [17].

We have also performed the calculations with LSDA+U for the P and AP alignments of Ru and Mn in the $I4/mcm$ configuration of $SrRu_{0.75}Mn_{0.25}O_3$. The total energy of the FM coupling of Mn and Ru is lower than the AFM coupling in the LSDA+U calculation in contrast to the LSDA calculation. As shown in Figs. 6(a)–(d), there

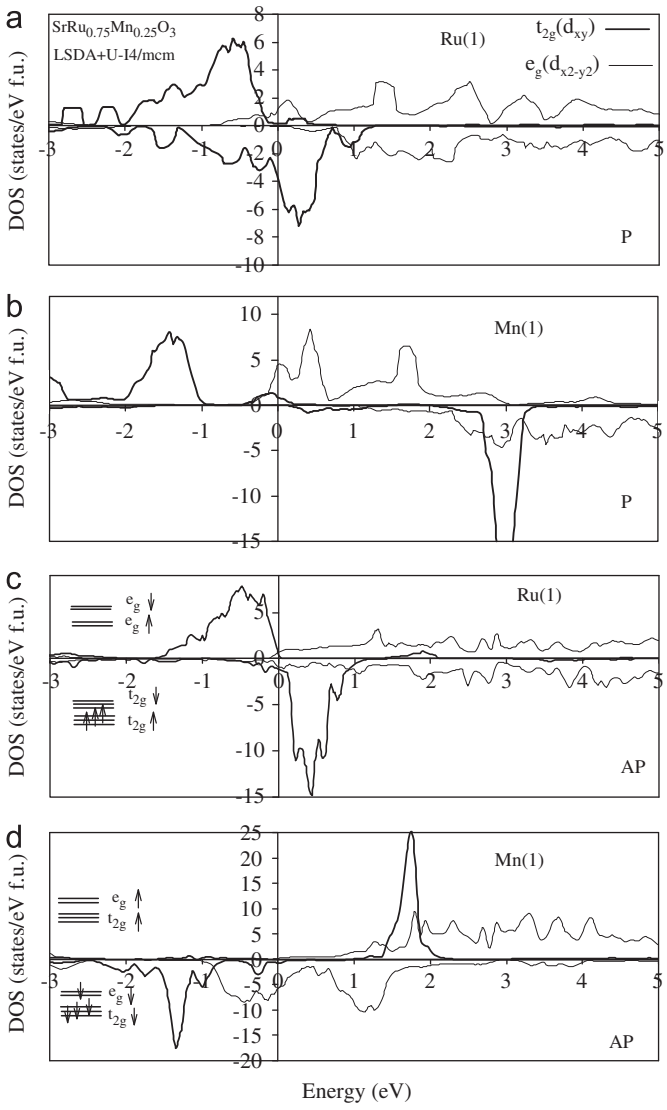

Fig. 6. DOS (d_{xy} and $d_{x^2-y^2}$) calculated by LSDA+U for $SrMn_{0.25}Ru_{0.75}O_3$ in the $I4/mcm$ space group: (a) DOS of Ru(1) in the parallel alignment of Ru and Mn moments (P), (b) DOS of Mn(1) in the parallel alignment of Ru and Mn moments (P), (c) DOS of Ru(1) in the antiparallel alignment of Ru and Mn moments (AP), (d) DOS of Mn(1) in the antiparallel alignment of Ru and Mn moments (AP). The DOS results are presented for the two up- and down-spins.

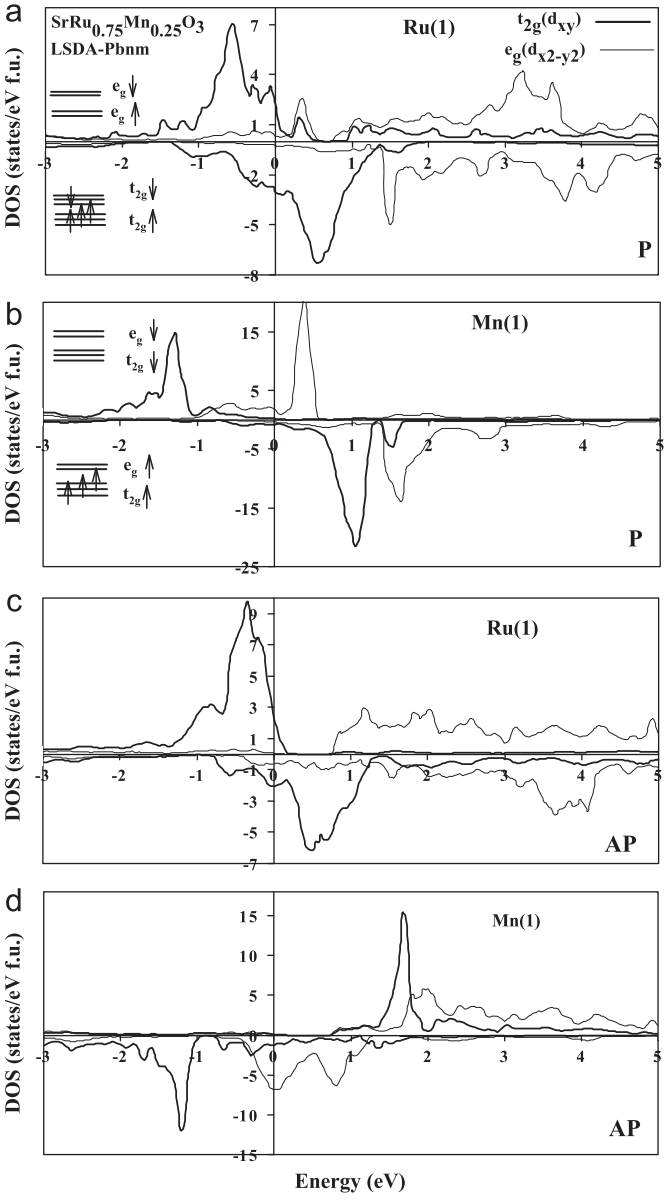

Fig. 7. DOS (d_{xy} and $d_{x^2-y^2}$) calculated by LSDA for $SrMn_{0.25}Ru_{0.75}O_3$ in the $Pbnm$ space group: (a) DOS of Ru(1) in the parallel alignment of Ru and Mn moments (P), (b) DOS of Mn(1) in the parallel alignment of Ru and Mn moments (P), (c) DOS of Ru(1) in the antiparallel alignment of Ru and Mn moments (AP), (d) DOS of Mn(1) in the antiparallel alignment of Ru and Mn moments (AP). The DOS results are presented for the two up- and down-spins.

is no significant difference in the topology of Ru and Mn DOS and electronic parameters as compared with the LSDA calculation. As shown in Tables 2 and 3, with the presence of Mn in the compound, the E_{ES} and magnetic moment of Mn electrons increase sharply. The LSDA+U calculation shows that Coulomb correlation can play an important role in the electronic structure of $SrRu_{0.75}Mn_{0.25}O_3$, but substitution of Mn for Ru adds small Coulomb correlation into the system due to screening of Mn electron in the Ru host system. Our LSDA+U calculation results (large U) is not relevant to the low Mn-doping with the itinerant electron (small U); and the LSDA result is sufficient to describe the electronic structure of the low Mn-doping.

3.1.2. Orthorhombic single crystal samples of $SrRu_{0.75}Mn_{0.25}O_3$

The total energy of the *Pbnm* configuration with P coupling of Mn and Ru (Figs. 7(a) and (b)) is very close to the AP alignment coupling (Figs. 7(c) and 7(d)) and has lower energy about 0.05 eV, which is assumed to be the ground state. This result is consistent with the QCP between the FM and AFM in single crystals which shows the FM coupling below $x=0.39$ [17]. The DOS (Figs. 7(a) and (b)) of P alignment phase for the *Pbnm* symmetry is very similar to the one for the *I4/mcm* symmetry. Both the Ru and Mn valances are near to +4 with small amount of Mn^{3+} and Ru^{5+} which is consistent with the experimental results [17]. As shown in Figs. 8(a) and (b), due to more electron contribution of different Mn e_g orbitals at Fermi level, there is more Ru–Mn charge transfer in the AP alignment calculation (from Ru 4e in $x=0$ to Ru 3.5e in $x=0.25$) as compared to the P alignment calculation (from Ru 4e in $x=0$ to Ru 3.7e in $x=0.25$). So, the P alignment *Pbnm* calculation suggests that in spite of the low Mn–Ru charge transfer, the existence of the mixed valance state (Mn^{3+}/Mn^{4+} and Ru^{4+}/Ru^{5+}) introduces a DE interaction which results in a FM coupling between the Mn ions.

As mentioned before, the unit cell volume reduces with increasing x, which is associated with a smaller ionic radii of Mn^{4+} than Ru^{4+}. From the neutron diffraction measurements of $SrRu_{1-x}Mn_xO_3$, the

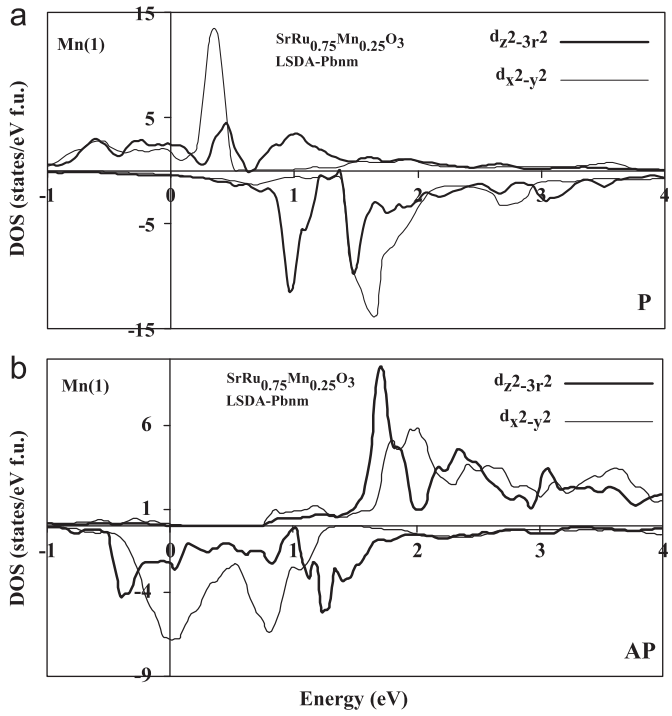

Fig. 8. DOS Mn 3*d* e_g orbitals calculated by LSDA for $SrMn_{0.25}Ru_{0.75}O_3$ in the *Pbnm* space group: (a) DOS of $d_{z^2-3r^2}$ and $d_{x^2-y^2}$ in the parallel alignment of the Ru and Mn moments (P), (b) DOS of $d_{z^2-3r^2}$ and $d_{x^2-y^2}$ in the antiparallel alignment of the Ru and Mn moments (AP).

Table 4
Electronic parameters for the *Pbnm* $SrRu_{0.75}Mn_{0.25}O_3$ perovskites deduced by DOS: magnetic moment (MM), orbital occupancy (OO), total energy (*E*).

Formula (approximation)	Ru(MM) (μ_B)	Mn(MM) (μ_B)	Ru(OO) (e)	Mn(OO) (e)	*E* (eV)
$SrRu_{0.75}Mn_{0.25}O_3$ (P-LSDA)	1.26	2.9	3.7	3.4	0.00
$SrRu_{0.75}Mn_{0.25}O_3$ (AP-LSDA)	1.26	−3.22	3.5	3.8	0.05

unit-cell volume exhibits deviations from the linear behavior of the Vegard law with increasing *x* in the tetragonal polycrystalline samples [24]. These deviations can be explained by considering the charge transfer $Ru^{4+}+Mn^{4+}\rightarrow Ru^{5+}+Mn^{3+}$. By comparing the stable magnetic phases in the polycrystalline and single crystal samples, as shown in Tables 3 and 4, respectively, it is found that the spin magnetic moment centered at the Ru sites in the P alignment *Pbnm* is about $1.26\mu_B$, which is large compared to the Ru magnetic moment of AP alignment *I*4/*mcm* (≈ 1.06). Also, the Ru t_{2g} and e_g DOS calculations (Fig. 4(c)), which is consistent with the magnetic moment of these atoms, suggest more charge transfer from Ru to Mn in the *I*4/*mcm* as compared to the *Pbnm* symmetry (Fig. 7(a)). So, the structural phase transition from *Pbnm* (layered system) to *I*4/*mcm* (quasicubic systems) in the polycrystalline system not only increases the dimensionality of the Mn-doped $SrRuO_3$, but also enhances both the Ru–Ru connectivity and FM coupling in the systems.

3.2. High Mn-doping

For $SrRu_{0.5}Mn_{0.5}O_3$, we first compare the two P and AP alignment phases only in the tetragonal *I*4/*mcm* symmetry by LSDA approximation, and later will point out the difference between the results from the LSDA+*U* (correlated) and LSDA calculation. We have also carried out some calculations with the *Pbnm* symmetry, but the topology of the calculated DOS is similar to the *I*4/*mcm* results. The Mn–Ru AFM state for the high Mn-doping in the both tetragonal and orthorhombic symmetries are more energetically favorable than the FM ordering. The electronic structure for the 50% Mn supercell with FM and AFM alignments of Mn and Ru for the *I*4/*mcm* symmetry with LSDA calculation are shown in Figs. 9(a), (b) and (c), (d), respectively. In all calculations for $x=0.5$, the Ru t_{2g} bandwidths are noticeably suppressed from $W=2.2$ to 1.0 eV due to the reduced overlaps among the electron clouds.

The AP alignment DOS calculation (Figs. 9(c) and (d)) predicts that the Ru and Mn valence is closer to $4d^3$ Ru^{5+} and $3d^4$ Mn^{3+}, respectively than the P alignment calculation (Figs. 9(a) and (b)). This may suggest that some Ru^{4+} ions are promoted to Ru^{5+} to satisfy the charge neutrality. There is apparently more charge transfer between Mn and the Ru host in the AP alignment calculation (from Ru 4e in $x=0$ to Ru 3.2e in $x=0.5$) as compared to the P alignment case (from Ru 4e in $x=0$ to Ru 3.5e in $x=0.5$) which is consistent to the high Mn doping of PES spectra [19].

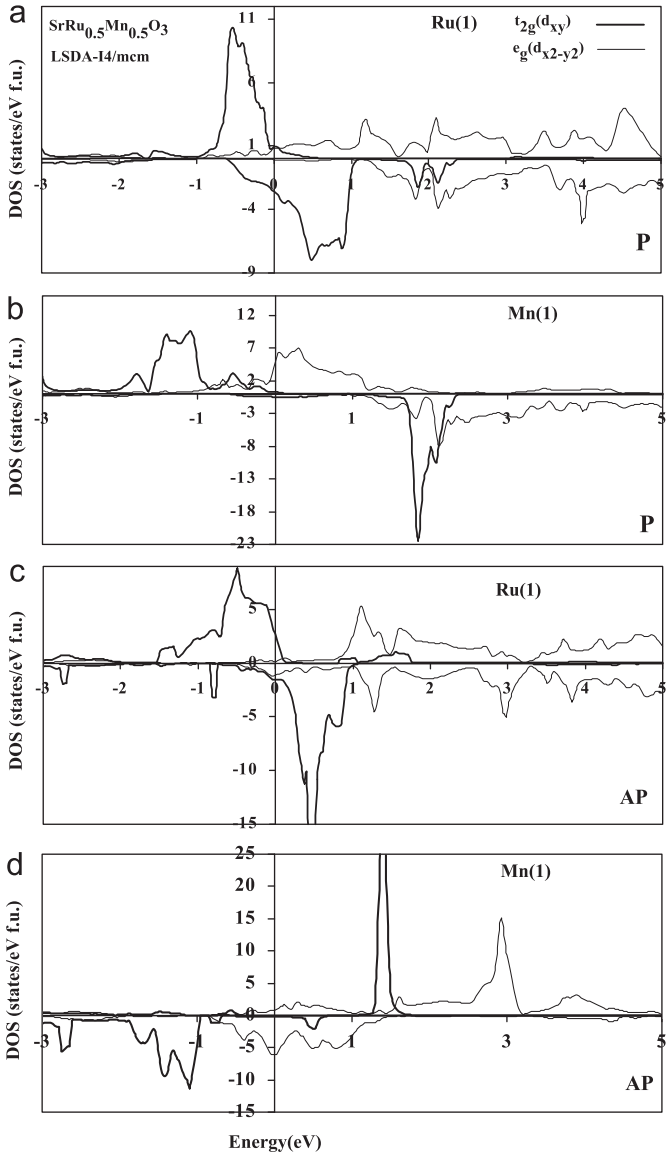

Fig. 9. DOS (d_{xy} and $d_{x^2-y^2}$) calculated by LSDA for $SrMn_{0.5}Ru_{0.5}O_3$ in the *I*4/*mcm* space group: (a) DOS of Ru(1) in the parallel alignment of Ru and Mn moments (P), (b) DOS of Mn(1) in the parallel alignment of Ru and Mn moments (P), (c) DOS of Ru(1) in the antiparallel alignment of Ru and Mn moments (AP), (d) DOS of Mn(1) in the antiparallel alignment of Ru and Mn moments (AP). The DOS results are presented for the two up- and down-spins.

This orbital occupancy is consistent with the results of the magnetic moment calculation of the AP alignment phase. The discrepancy between LSDA calculation for $x=0.5$ and insulator phase in experiment indicates that the electron correlation plays an important role in the metal–insulator transition mechanism.

Substituting Ru by Mn replaces four itinerant 4*d* electrons with three localized 3*d* electrons. Due to the small spatial extent of the 3*d* orbitals in the high Mn-doping, the electron–electron correlation effect becomes important. So, we now explicitly add the correlation effects into our electronic structure calculations for $SrRu_{0.5}Mn_{0.5}O_3$. Fig. 10 illustrates the Ru and Mn DOS of $SrRu_{0.5}Mn_{0.5}O_3$ from the LSDA+*U* calculations with $U=5.5$ eV for Mn ($U=1.5$ eV for Ru) for the P (Figs. 10(a) and (b)) and AP alignment (Figs. 10(c) and (d)) phases. The LSDA+*U* calculation shows enhancement of the both Ru and Mn magnetic moment as compared to the LSDA calculation; the magnetic moment per atom is found to be 1.64 and $3.33\mu_B$/Mn for P alignment calculation, which is consistent with the presence of Ru^{5+} and Mn^{3+}. The bigger E_{ES} of Ru 4*d* and Mn 3*d* at Fermi level in the LSDA+*U* calculation (Figs. 10(a) and (b)) compared with that of LSDA calculation (Figs. 9(a) and (b)) shows the essential role of correlation in determining the electronic structure of this compound.

As shown in Fig. 10(d), for high values of *x*, in the ground state AP alignment calculation, the Mn valances is similar to the magnetic moment of purely ionic compound and also $SrMnO_3$ (Fig. 3(b)) with d^3 configuration. Therefore, substitution of Mn leads to the formation of AFM Mn^{4+}–O–Mn^{4+} and Ru^{5+}–O–Mn^{4+} insulating arrangement similar to Ref. [28]. Also, substitution of Mn for the Ru destroys the ordering of both Mn^{3+}–O–Mn^{4+} ions and Ru^{5+}–O–Mn^{3+} which are necessary to enhance the FM ordering. The change of charge valance due to substitutions of impurity (hybridization between impurity atom and host) induces exchange splitting which is responsible for high Curie temperature in the system as discussed for the Sr_2FeMoO_6 and $Cr_xRu_{1-x}SrO_3$ compounds. This mechanism works in the low impurity-doping of Mn in $Mn_xRu_{1-x}SrO_3$ and also for the compound mentioned above. In the high impurity doping regime, the antiferromagnetic interaction between Mn atoms is dominant and superexchange between Mn atoms is responsible for antiferromagnetic coupling in the system.

For AP alignment calculations, compared with LSDA, the correlated bands are narrower and the inclusion of correlations causes a sharp drop in the DOS at the Fermi level. The contribution of the Ru 4*d* and Mn 3*d* states is completely vanished at fermi level for both up-spin and down-spin channel; and the material is an insulator with the energy gaps of 1.2 eV (Fig. 10(c)). This significantly increases the magnetic moment of Mn to around $-3.4\mu_B$, and enhances the E_{ES} of the Ru 4*d* states to 4.8 eV as compared to 2.80 eV in LSDA (Table 2). Also, crystal electric field gap at E_F in the up-spin channel is enhanced between the occupied Ru t_{2g} and the empty Ru e_g bands. Completely eliminating of one electron in the Ru 4*d* interrupt the itinerancy of the Ru electrons by substitution of 50% of Mn^{4+} for Ru^{4+}. The metallic and FM behavior of $SrRu_{1-x}Mn_xO_3$ disappears with increasing *x* up to 0.5. So, the computational results described in the last section for the low Mn-doing tetragonal polycrystalline structure and this section for the high Mn-doping predicts the experimental results suggested by Ref. [24] with spin glass behavior for the intermediate range and the AFM coupling for the high doping case.

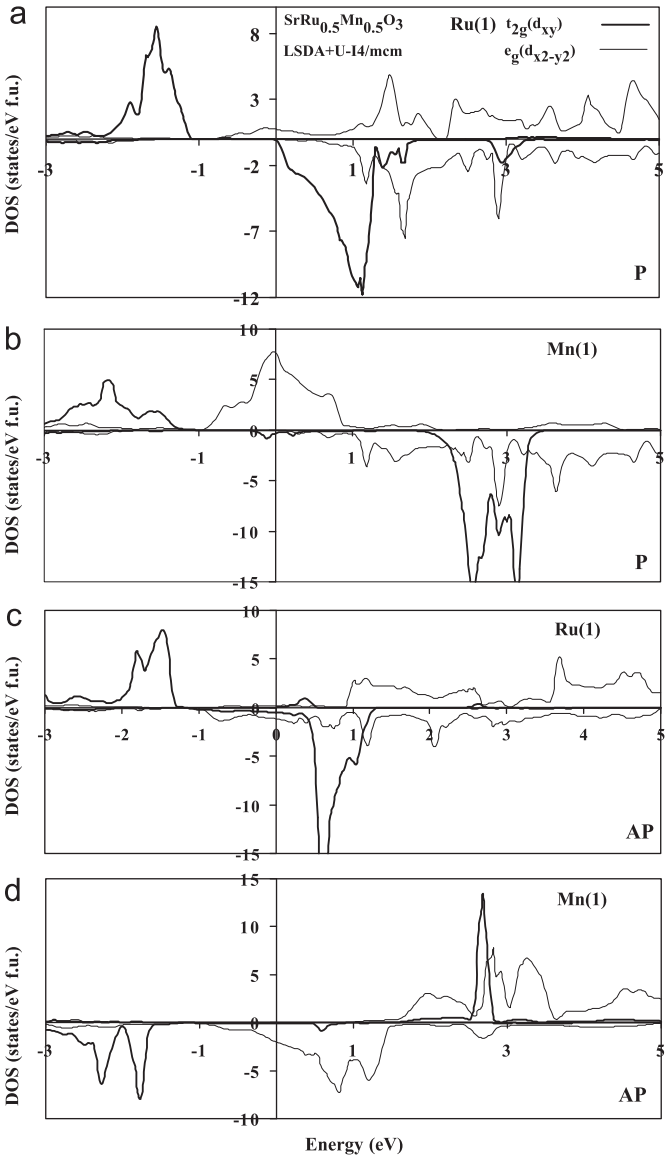

Fig. 10. DOS (d_{xy} and $d_{x^2-y^2}$) calculated by LSDA+U for $SrMn_{0.5}Ru_{0.5}O_3$ in the *I*4/*mcm* space group: (a) DOS of Ru(1) in the parallel alignment of Ru and Mn moments (P), (b) DOS of Mn(1) in the parallel alignment of Ru and Mn moments (P), (c) DOS of Ru(1) in the antiparallel alignment of Ru and Mn moments (AP), (d) DOS of Mn(1) in the antiparallel alignment of Ru and Mn moments (AP). The DOS results are presented for the two up- and down-spins.

4. Summary

The appearance of magnetic transition in $SrRu_{1-x}Mn_xO_3$ show that these compounds is sensitive to the conditions of sample preparation, which produces different magnetic interactions between the Mn and Ru moments. For the low Mn-doping of the polycrystalline sample with tetragonal symmetry, by substituting Ru by Mn in $SrRuO_3$, the AFM coupling between Mn and Ru becomes stable, and all the *d* states with large exchange interaction then renormalize due to hopping between Ru and Mn. This AFM coupling between Mn and Ru host lattice aligns the Ru moments and provides an explanation for retaining the high Curie temperature of $SrRuO_3$ with Mn substitution. The formation of AFM alignment agrees with the coexistence of ferromagnetism and antiferromagnetism. The DOS and magnetic moment results show the presence of Ru^{5+} ions in these polycrystalline materials. The situation is reversed for the orthorhombic single crystal samples with substitution of Mn for Ru. The FM ground state and creation of both Ru^{4+} and Mn^{4+} in the *Pbnm* orthorhombic phase is consistent with the QCP between FM and AFM transitions in the single crystal system. In the high Mn-doping, the LSDA+*U* calculation with AFM ordering show that the electron–electron correlation plays an important role in predicting the insulating

behavior of these materials. The DOS and the calculated magnetic moment of Mn is similar to the magnetic moment of purely ionic compound with d^3 configuration. So, the computational results described in the low Mn-doing and for high Mn-doping simulates both the experimental results suggested in Ref. [24] with the spin glass behavior and also the phase diagram with QCP in Ref. [17] with constructing the tetragonal and orthorhombic phases.

Acknowledgments

We would like to acknowledge fruitful discussions with H. Khosroabadi and R. Mozaffari. This work was supported in part by the Office of the Vice President of Research, and the National Centre of Excellence in Complex Systems and Condensed Matter (CSCM) of the Department of Physics at Sharif University of Technology (http://www.cscm.ir).

References

[1] H.-T. Jeng, S.-H. Lin, C.-S. Hsue, Phys. Rev. Lett. 97 (2006) 067002.
[2] J.S. Ahn, J. Bak, H.S. Choi, T.W. Noh, J.E. Han, Y. Bang, J.H. Cho, Q.X. Jia, Phys. Rev. Lett. 82 (1999) 5321.
[3] A.V. Puchkov, M.C. Schabel, D.N. Basov, T. Startseva, G. Cao, T. Timusk, Z.-X. Shen, Phys. Rev. Lett. 81 (1998) 2747.
[4] D.A. Crandles, M.M. Yazdanian, F.S. Razavi, J. Phys. D: Appl. Phys. 39 (2006) 6.
[5] A.D. Crandles, M. Reedyk, R.W. Schaeffer, A.E. Hultgren, R. Schlee, Phys. Rev. B 65 (2002) 224407.
[6] A. Mamchik, I.-W. Chen, Phys. Rev. B 70 (2004) 104409.
[7] K.W. Kim, J.S. Lee, T.W. Noh, S.R. Lee, K. Char, Phys. Rev. B 71 (2005) 125104.
[8] P.-A. Lin, H.-T. Jeng, C.-S. Hsue, Phys. Rev. B 77 (2008) 085118.
[9] A. Gupta, B.W. Hussey, T.M. Shaw, Mater. Res. Bull. 31 (1996) 1463.
[10] L. Mieville, T.H. Geballe, L. Antognazza, K. Char, Appl. Phys. Lett. 70 (1997) 126.
[11] L. Pi, A. Maignan, R. Retoux, B. Raveau, J. Phys.: Condens. Matter 14 (2002) 7391.
[12] B. Dabrowski, S. Kolesnik, O. Chmaissem, T. Maxwell, M. Avdeev, P.W. Barnes, J.D. Jorgensen, Phys. Rev. B 72 (2005) 054428.
[13] V. Durairaj, S. Chikara, X.N. Lin, A. Douglass, G. Cao, P. Schlottmann, E.S. Choi, R.P. Guertin, Phys. Rev. B 73 (2006) 214414.
[14] Z.H. Han, J.I. Budnick, W.A. Hines, B. Dabrowski, S. Kolesnik, T. Maxwell, J. Phys.: Condens. Matter 17 (2005) 1193.
[15] A.J. Williams, A. Gillies, J.P. Attfield, G. Heymann, H. Huppertz, M.J. Martinez-Lope, J.A. Alonso, Phys. Rev. B 73 (2006) 104409.
[16] G. Cao, S. McCall, M. Shepard, J.E. Crow, R.P. Guertin, Phys. Rev. B 56 (1997) 321.
[17] G. Cao, S. Chikara, X.N. Lin, E. Elhami, V. Durairaj, P. Schlottmann, Phys. Rev. B 71 (2005) 035104.
[18] R.K. Sahu, S.S. Manoharan, J. Appl. Phys. 92 (2002) 4831.
[19] K. Horiba, H. Kawanaka, Y. Aiura, T. Saitoh, C. Satoh, Y. Kikuchi, M. Yokoyama, Y. Nishihara, R. Eguchi, Y. Senba, H. Ohashi, Y. Kitajima, S. Shin, Phys. Rev. B 81 (2010) 245127.
[20] Y. Maeno, H. Hashimoto, K. Yoshida, S. Nishizaki, T. Fujita, J.G. Bednorz, F. Lichtenberg, Nature (London) 372 (1994) 532.
[21] P. Khalifah, I. Ohkubo, H. Christen, D. Mandrus, Phys. Rev. B 70 (2004) 134426;
Y.S. Lee, J. Yu, J.S. Lee, T.W. Noh, T.H. Gimm, H.Y. Choi, C.B. Eom, Phys. Rev. B 66 (2002) 041104(R).
[22] T. Takeda, S. Ohara, J. Phys. Soc. Jpn. 37 (1974) 275.
[23] O. Chmaissem, B. Dabrowski, S. Kolesnik, J. Mais, D.E. Brown, R. Kruk, P. Prior, B. Pyles, J.D. Jorgensen, Phys. Rev. B 64 (2001) 134412.
[24] S. Kolesnik, B. Dabrowski, O. Chmaissem, Phys. Rev. B 78 (2008) 214425.
[25] T. He, Q. Huang, R.J. Cava, Phys. Rev. B 63 (2001) 024402.
[26] R.K. Sahu, Z. Hu, M.L. Rao, S.S. Manoharan, T. Schmidt, B. Richter, M. Knupfer, M. Golden, J. Fink, C.M. Schneider, Phys. Rev. B 66 (2002) 144415.
[27] X.-Y. Zhang, Y. Chen, Z.-Y. Li, C. Vittoria, V.G. Harris, J. Phys.: Condens. Matter 19 (2007) 266211.
[28] Y. Ying, J. Fan, L. Pi, Z. Qu, W. Wang, B. Hong, S. Tan, Y. Zhang, Phys. Rev. B 74 (2006) 144433.
[29] M. Yokoyama, C. Satoh, A. Saitou, H. Kawanaka, H. Bando, K. Ohoyama, Y. Nishihara, J. Phys. Soc. Jpn. 74 (2005) 1706.
[30] E. Sjostedt, L. Nordstrom, D.J. Singh, Solid State Commun. 114 (2000) 15;
G.K.H. Madsen, P. Blaha, K. Schwarz, E. Sjostedt, L. Nordstrom, Phys. Rev. B 64 (2001) 195134.
[31] K. Schwarz, P. Blaha, Comput. Mater. Sci. 28 (2003) 259.
[32] D. Singh, Phys. Rev. B 43 (1991) 6388.
[33] B.J. Kennedy, B.A. Hunter, Phys. Rev. B 58 (1998) 653.
[34] A.I. Liechtenstein, V.I. Anisimov, J. Zaanen, Phys. Rev. B 52 (1995) R5467;
V.I. Anisimov, F. Aryasetiawan, A.I. Lichtenstein, J. Phys.: Condens. Matter 9 (1997) 767.
[35] D.A. Papaconstantopoulos, W.E. Pickett, Phys. Rev. B 57 (12) (1997) 751;
J.H. Jung, K.H. Kim, D.J. Eom, T.W. Noh, E.J. Choi, J. Yu, Y.S. Kwon, Y. Chung, Phys. Rev. B 55 (15) (1997) 489.
[36] R. Søndena, P. Ravindran, S. Stølen, T. Grande, M. Hanfland, Phys. Rev. B 74 (2006) 144102.
[37] D. Kasinathan, D.J. Singh, Phys. Rev. B 74 (2006) 195106.
[38] D.D. Sarma, P. Mahadevan, T. Saha-Dasgupta, S. Ray, A. Kumar, Phys. Rev. Lett. 85 (2000) 2549.
[39] H. Hadipour, M. Akhavan, J. Solid State Chem. 183 (2010) 1678.